Mapping of Translating, Rotating Icebergs With an Autonomous Underwater Vehicle

Peter W. Kimball and Stephen M. Rock

Abstract—**This paper presents a method for mapping translating, rotating icebergs with an autonomous underwater vehicle (AUV). To map an iceberg, the AUV first circumnavigates it, collecting multibeam sonar ranges and iceberg-relative Doppler sonar velocities from the submerged iceberg surface. The primary challenge is then to estimate the trajectory of the mapping vehicle in a noninertial reference frame attached to the moving iceberg. The collected multibeam ranges may then be projected from this trajectory to form a map of the iceberg's submerged surface. The approach of the method involves identifying the iceberg-frame locations of all the Doppler sonar measurements made during circumnavigation, allowing the AUV's iceberg-relative trajectory to be computed from those locations. The measurement locations are estimated simultaneously with the trajectory of the iceberg to be most consistent with the inertial-space positions, inertial-space velocities, distances between points on the iceberg surface as measured by the Doppler sonar, and alignment of multibeam ranges measured at the beginning and end of the circumnavigation. The measurements depend nonlinearly on the modeled positions and iceberg trajectory, and the paper presents a solution formulation that deals efficiently with the nonlinearity. By incorporating iceberg-relative vehicle velocity into the estimation, the method achieves two significant advances beyond prior work by the authors. First, and most significantly, the method adds ice-relative vehicle velocity measurements (e.g., using a Doppler velocity logger). This makes the method robust to common vehicle inertial navigation errors. Second, inclusion of iceberg-relative vehicle velocity data allows for the identification of a more general model of iceberg trajectory, making the method robust to changes in iceberg translation and rotation rates. Currently, no iceberg circumnavigation data sets are available that include iceberg-relative velocity from Doppler sonar. However, this paper includes results from simulated free-drifting icebergs, and experimental results from an AUV seafloor mapping dive. The simulation data provide a moving iceberg testbed with known ground truth for the mapping results. The seafloor data provide a qualitative verification that the method works with real vehicle data.**

Index Terms—**Estimation , ice, marine navigation, marine vehicles, motion estimation, terrain mapping.**

Manuscript received February 11, 2013; revised September 30, 2013; accepted January 09, 2014. Date of publication February 21, 2014; date of current version January 09, 2015. This work was supported by the National Science Foundation and the National Aeronautics & Space Administration's Astrobiology Science and Technology for Exploring Planets Program.

Associate Editor: R. Eustice.

P. W. Kimball is with the Applied Ocean Physics & Engineering Department, Woods Hole Oceanographic Institution, Woods Hole, MA USA (e-mail: pkimball@whoi.edu).

S. M. Rock is with the Department of Aeronautics and Astronautics and the Aerospace Robotics Laboratory, Stanford University, Stanford, CA 94305 USA.

Digital Object Identifier 10.1109/JOE.2014.2300396

I. Introduction

THIS paper presents a technique for creating 3-D maps of the submerged surfaces of free-drifting icebergs using an autonomous underwater vehicle (AUV). There is growing interest in the scientific community to understand the impact of large, free-drifting icebergs on ocean ecosystems and global energy processes. AUVs present an opportunity for very high spatial and temporal resolution sampling around icebergs (compared to other existing sampling techniques). Prior work has identified maps of free-drifting icebergs as both an important scientific data product and an enabler of close-proximity iceberg-relative AUV navigation [12]. Existing AUV mapping techniques are well developed for seafloor applications, but require extension to handle the noninertial motion (translation and rotation) of free-drifting icebergs.

The map surface data in this application come from a multibeam sonar carried by a submerged AUV. As the AUV drives around an iceberg, this instrument collects a 2-D, cross-track fan-shaped pattern of hundreds of range measurements from the vehicle to the iceberg's submerged surface once every 1–3 s. A map of the iceberg is formed by projecting these multibeam ranges from a best estimate of the iceberg-relative vehicle position and orientation at the time of each measurement, i.e., a reconstructed vehicle trajectory in an iceberg-fixed frame. This reference frame is noninertial, translating and rotating with the iceberg. Estimating the AUV trajectory in this frame is the focus of this paper.

Iceberg translation and rotation through inertial space are significant during the time required for an AUV to travel around an iceberg and achieve multibeam sonar coverage. Iceberg translational speeds of 0.03–0.08 m/s and rotation rates of 5–10°/h are typical, while translational speeds up to 0.27 m/s and rotation rates up to 40°/h have been observed [18], [8]. Even for a relatively fast AUV with a nominal operating speed of 1.75 m/s, circumnavigating a small (1.8 km across) iceberg takes an hour. Typical iceberg motion over this time can result in 110–290 m of accumulated displacement, and 5°–10° of orientation change.

Prior iceberg mapping work by the authors [12] demonstrates the need to account for iceberg motion to create self-consistent iceberg maps. It utilizes a simple, constant-translation, constant-rotation model of iceberg motion and identifies the parameter values in the model only through loop closure in the multibeam data, i.e., the translation and rotation rates are chosen to maximize self-consistency in the map region ensonified both at the beginning and end of the circumnavigation. That work does not include any direct measurements of iceberg-relative vehicle velocity from Doppler sonar.

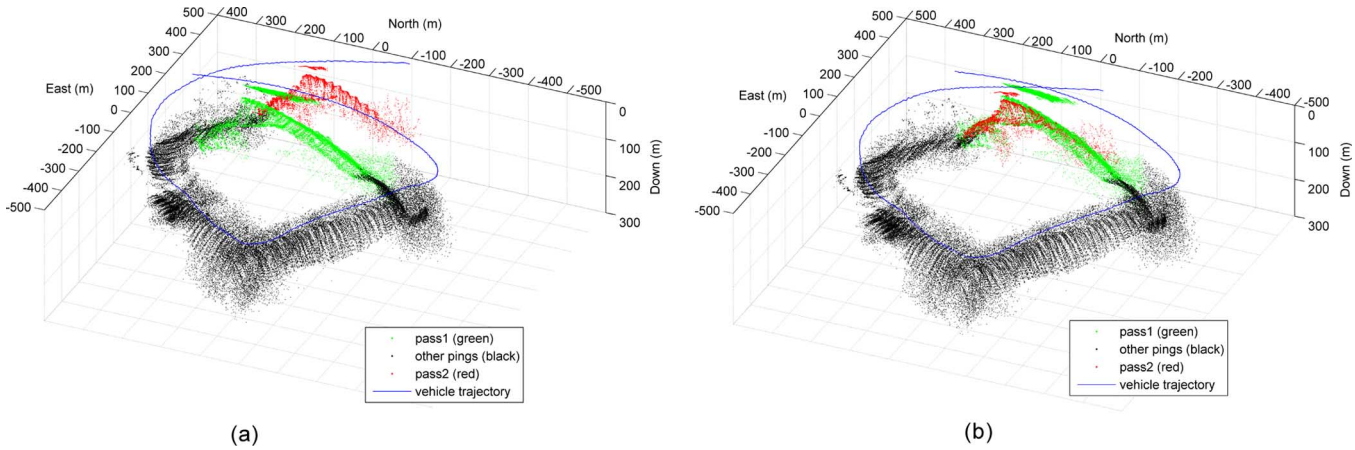

Fig. 1. Iceberg mapping results from [12]. The mapping vehicle's iceberg-relative trajectory is estimated using a constant-velocity model for iceberg motion to achieve self-consistency in a twice-scanned region the map. (a) Map created by projecting sonar ranges from vehicle's inertial-space trajectory. (b) Map created by projecting sonar ranges from vehicle's iceberg-relative trajectory.

Fig. 1 shows a mapping result from [12] in which ship-based, sideways-looking multibeam sonar data collected during circumnavigation of a small Antarctic iceberg are projected from the Global Positioning System (GPS) trajectory of the ship. Overlapping multibeam ranges from the beginning and end of the circumnavigation are shown in green and red, respectively. Fig. 1(a) illustrates the inconsistency of a map created without accounting for iceberg motion, i.e., by projecting the multibeam ranges from the vehicle's unmodified inertial-space trajectory. Fig. 1(b) illustrates that a self-consistent map may be achieved through the addition of a simple iceberg motion model, i.e., by subtracting the estimated iceberg trajectory from the GPS-measured vehicle trajectory to obtain the trajectory of the vehicle in an iceberg-fixed frame, and finally projecting the multibeam ranges from that iceberg-relative trajectory. The constant-velocity, constant-rotation iceberg motion model accounts for the total displacement and rotation of the iceberg during data collection, and is sufficient to create a self-consistent iceberg map.

The extended formulation in this paper differs most significantly from [12] in that it incorporates ice-relative AUV velocity measurements from a Doppler velocity logger (DVL). With these measurements, the extended formulation overcomes two significant shortcomings of the original, inertial-navigation-only technique:

First, and most significantly, mapping results from the inertial-navigation-only technique depend entirely upon the quality of the vehicle's inertial navigation. Enforcing loop closure "ties together" the two ends of the trajectory (and their associated projected sonar ranges), but the vehicle's inertial navigation is the only source of information about the iceberg shape between the endpoints—errors in the measurement of vehicle's inertial-space trajectory translate directly into errors in the iceberg map. The ship-based demonstration in [12] uses high-quality GPS measurement of the vehicle's inertial-space trajectory, but precise inertial navigation of AUVs in deep water (where bottom lock is not possible) is a difficult problem. Accelerometer dead reckoning alone gives very poor accuracy. Accurate solutions require the addition of water-relative velocity dead reckoning, frequent GPS (surface) fixing, and/or external acoustic aiding. These techniques are significantly complicated and often impossible around free-drifting icebergs. In the extended formulation in this paper, DVL provides a direct, high-quality measurement of iceberg-relative vehicle trajectory (so long as the vehicle heading may be measured accurately, and the iceberg heading may be estimated accurately)—making the mapping results robust to poor-quality vehicle inertial navigation.

Second, the constant-rate iceberg motion model cannot account for any changes in iceberg translation or rotation rates over the course of data collection. Any difference between the true iceberg motion and the modeled iceberg motion results in warpage of the iceberg map. The DVL measurements in the present method allow a variable-rate spline model of iceberg motion to be identified, reducing map warpage in cases of time-varying iceberg rates. See [15] for a documented example of an iceberg trajectory with rapidly varying rates.

Fig. 2 shows the concept of an AUV collecting both multibeam and DVL sideways-looking sonar measurements while circumnavigating an iceberg. The approach of the method is to identify the iceberg-frame locations of all the DVL measurements made during circumnavigation, allowing the AUV's iceberg-relative trajectory to be computed from those locations. The measurement locations are estimated simultaneously along with the trajectory of the iceberg, since the available measurements depend on both. The estimation is posed as a large (thousands of parameters) multiobjective least squares minimization that chooses the DVL measurement locations and iceberg trajectory that are most consistent with the collected measurements. Note that because the important loop-closure information is not available until the vehicle has driven completely around the iceberg, the applicability of online recursive simultaneous localization and mapping (SLAM) techniques is limited. The estimation of iceberg-frame measurement locations and inertial-space iceberg trajectory is performed here as a batch, postprocessing operation—a form of offline SLAM.

Section II presents related work in underwater terrain mapping, and robotic mapping in noninertial reference frames. Section III details the iceberg shape and trajectory estimation formulation as well as a solution technique that handles the nonlinear dependence of available measurements upon the

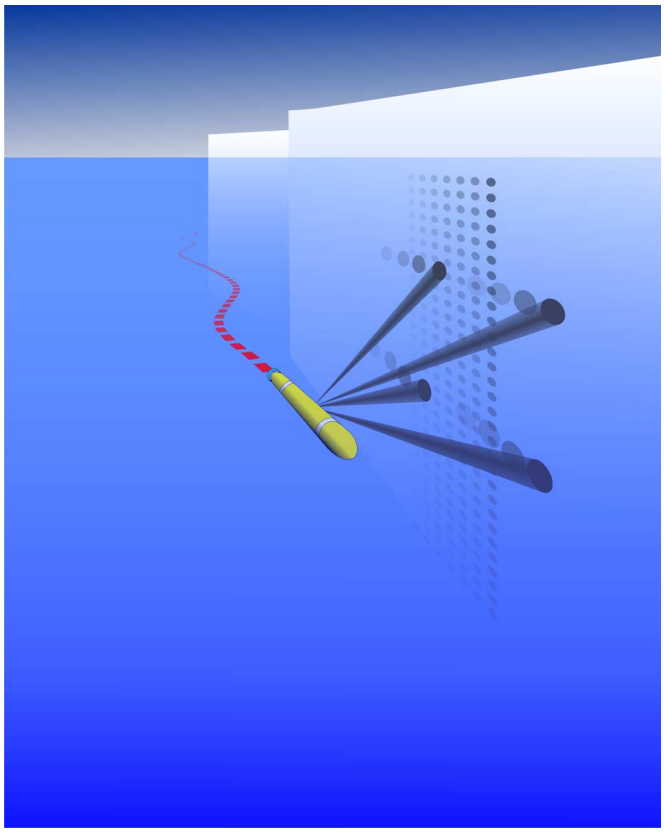

Fig. 2. AUV with sideways-looking four-beam DVL and multibeam sonar footprints shown.

quantities to be estimated. Section IV-B presents mapping results from simulated free-drifting icebergs, and from real AUV data using the seafloor as an iceberg surrogate with known stationary trajectory. Section V concludes the paper.

II. Background

A. Terrain Mapping

Published bathymetric maps are created by casting recorded sonar ranges from a best estimate of the trajectory in space from which they were collected. The sonar data used to create these maps can be collected from ship-mounted systems or from submerged vehicles such as towfish, remotely operated vehicles (ROVs), and AUVs. The advantage of submerged vehicles is that they can produce data of higher resolution due to their proximity to the seafloor. In either case, generating the map requires an accurate estimate of the vehicle's trajectory. For ship-based systems creating maps of the seafloor, this is relatively straightforward since the trajectory of the ship can be measured accurately using GPS.

Submerged vehicles are unable to use GPS positioning, and best estimates of submerged vehicle trajectories must be formed in other ways. Dead-reckoned inertial navigation forms the starting point for these techniques, but is subject to accumulated error (i.e., drift). There are two common techniques for overcoming dead-reckoning error to achieve a best estimate of an underwater vehicle's trajectory during mapping operations. One is to use deployed and surveyed long-baseline acoustic arrays for vehicle position measurement (e.g., in [7] and [19], and in the Arctic [10]). The other is to exploit self-intersecting trajectories and use terrain correlation at these intersection points to perform adjustments to the estimated vehicle trajectory in postprocessing (e.g., [13] and [17]). Both approaches can provide maps of meter-level accuracy. Generally, acoustic array methods may give lower map georeferencing errors, while use of terrain correlation may give superior local consistency.

Due to the difficulty of installing an acoustic array on an iceberg, surveying it into a reference frame attached to the iceberg, and reliably interrogating it from an AUV, neither the method in [12] nor the extended method in this paper utilizes acoustic arrays for iceberg-relative navigation. However, like terrain-correlation seafloor mapping techniques, they both use loop closure identified in multibeam ranges at the beginning and end of the circumnavigation to identify the best estimate terrain-relative mapping vehicle trajectory. The extended formulation also incorporates iceberg-relative vehicle velocity measurements to identify the best estimate mapping vehicle trajectory.

B. Robotic Mapping in Noninertial Reference Frames

There is a vast literature on SLAM, relative pose estimation, and 3-D reconstruction. However, as discussed in [1], most of this work deals with static targets or environments. Robotic mapping within noninertial reference frames is still an emerging family of problems.

In [1], a chaser vehicle forms a map of 3-D feature locations on a moving target (e.g., tumbling spacecraft or moored instrument) undergoing unknown forces and moments. The hybrid Bayesian/optimization approach uses discrete feature locations identified in successive camera images of the target. This work is not portable to the problem of mapping large environments such as icebergs because it requires successive camera views large enough to include multiple repeatably identifiable features on the target to estimate target motion and target shape simultaneously. Augenstein and Rock [1] illustrate the importance and role of constraints on the estimated motion of the mapping target.

Prior work with AUV navigation beneath moving ice, including [2], involves ice-relative sensing, such as ice-relative velocity from a DVL, and ice-relative position derived from beacons installed on the ice. These techniques have neither measured nor estimated ice-relative vehicle heading, and have therefore been subject to dead-reckoning errors due to ice rotation. These errors limit the applicability of the techniques to mapping applications in which ice rotation is negligible.

In 1985, the Dynamics of Iceberg Grounding and Scouring (DIGS) experiment deployed acoustic beacons and radar targets via a floating lasso around the perimeters of some small icebergs. These beacons and targets were used to determine the iceberg-relative position of a scanning sonar lowered from a ship to map icebergs [5]. This approach completely eliminates iceberg translation from the problem since iceberg-relative position of the sensors is measured directly via the beacons. No iceberg-relative heading information was available, so the sonar profiles had to be aligned in postprocessing. The DIGS program identified the lassoing process as an intricate one even for small icebergs during calm conditions, and identified the inability to

localize the transponders within the iceberg frame as a significant source of error.

Only the prior work by the authors [12] and AUV-based upward-looking sonar mapping of a rotating ice floe in [14] have relied on both ice-relative and inertial sensing, accounting explicitly for ice rotation in inertial space. In the latter, direct measurements of the ice floe's rotation and translation are obtained via the instrumentation of a ship moored to the floe during AUV operations. Those measurements are included in a pose-graph formulation of the mapping problem which estimates both the rotation of the floe and the floe-relative pose of the AUV at the time of every multibeam measurement.

The method presented in this work requires neither the installation of beacons on the iceberg nor the direct measurement of iceberg heading.

III. Method

A. Determining the Iceberg-Relative AUV Trajectory

The goal of the method is to estimate the mapping AUV's circumnavigation trajectory in a frame attached to the moving iceberg. From this trajectory, the collected multibeam ranges may be projected to form an iceberg map.

Each DVL measurement consists of the range and Doppler shift along each of four geometrically diverse beams (as in Fig. 2). Most DVL applications involve computing a single 3-D vehicle velocity based on the Doppler shifts measured along all four beams. This is understood as the velocity of the vehicle with respect to the seafloor in seafloor applications, and as the velocity of the vehicle with respect to the iceberg in this application.

Together with the vehicle's inertial-space velocity, the iceberg-relative velocity from DVL gives a measurement of the iceberg's inertial-space velocity. Because all points on the iceberg are moving with different velocities through inertial space (due to rotation), any iceberg velocity measured in this way applies only to a single point on the iceberg surface. In this method, that point is located on a plane fit to the four return locations, and along a ray in the center of the four-beam constellation (similar to one common practice for computing altitude using bottom-tracking DVLs). This single point is referred to as a "DVL projected point" (DPP) in the remainder of this paper. This approximation is only a very small source of error since the spread of the DVL beams is generally less than 50 m, a distance over which the difference in iceberg velocity due to rotation is negligible.

This method uses the iceberg-frame DPP locations and control points in a spline model of inertial-space iceberg trajectory as intermediate variables. The method chooses their values to maximize agreement with collected measurements, and then computes the iceberg-relative AUV trajectory from the estimated iceberg-frame DPP locations. Importantly, not all DVL measurements need to be assigned DPPs. As discussed in Section III-D3, most DVL measurements are used only as iceberg-relative vehicle velocity measurements for iceberg-relative dead reckoning, with DPPs computed from DVL measurements only every 100–200 m around the iceberg.

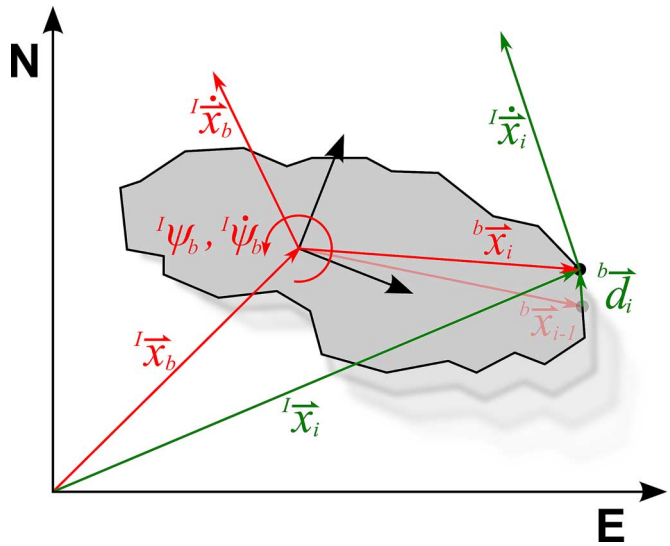

Fig. 3. Estimated quantities, shown in red, are chosen to be most consistent with measured quantities, shown in green. Estimated quantities include the position, velocity, rotation, and rotation rate of a frame attached to the iceberg as well as the positions in that frame of points ensonified by the DVL. Measured quantities include the inertial-space position and velocity of each point ensonified by the DVL, as well as its iceberg-frame distance from the previous ensonified point.

Computation of the AUV's iceberg-relative trajectory is straightforward once the DPP locations have been estimated: For each DPP location, the corresponding iceberg-frame AUV pose is computed from the associated DPP range measurement vector, oriented in the iceberg frame based on the estimated iceberg heading and measured vehicle orientation at the time of the measurement. Since DVL and multibeam measurements are generally asynchronous, vehicle poses at multibeam measurement times must then be computed by interpolation or intermediate dead reckoning.

B. DPP Locations

The iceberg-frame DPP locations and inertial-space iceberg trajectory spline control points are chosen to be most consistent with four types of measurements collected by the mapping AUV during a circumnavigation of the iceberg:

1) inertial-space position of each DPP;
2) inertial-space velocity of each DPP;
3) iceberg-frame distance between successive DPPs;
4) loop closure between DPPs in the beginning and end of the circumnavigation.

The first three are illustrated for a single DPP in Fig. 3 (loop closure is discussed separately in Section III-D4).

The DPP's position and velocity in inertial space ($^I\vec{x}_i$ and $^I\dot{\vec{x}}$) and the distance from the previous DPP in the iceberg frame ($^b\vec{d}_i$) are all measured by the vehicle's DVL and inertial navigation system. Those same quantities can be expressed in terms of the estimated iceberg-frame DPP locations and estimated inertial-space iceberg trajectory as well. The goal is to choose the estimated quantities (red in Fig. 3) to support the measured quantities (green in Fig. 3) as best as possible. Specifically, the

estimated iceberg trajectory and DPP positions are chosen to minimize

$$J = \|A_1\hat{\vec{x}} - {}^I\vec{x}\|^2 + \mu_2\|A_2\hat{\vec{x}} - {}^I\dot{\vec{x}}\|^2 + \mu_3\|A_3\hat{\vec{x}} - {}^b\vec{d}\|^2 + \mu_4\|A_4\hat{\vec{x}}\|^2 + \mu_5\|A_5\hat{\vec{x}}\|^2. \quad (1)$$

Each term of the cost function represents the disagreement between the model and one type of collected measurement. $\hat{\vec{x}}$ contains the control points for the iceberg translational trajectory spline, and the iceberg-frame DPP locations. $A_1\hat{\vec{x}}$ gives the modeled inertial-space DPP locations, and ${}^I\vec{x}$ contains the measured locations. $A_2\hat{\vec{x}}$ gives the modeled inertial-space DPP velocities, and ${}^I\dot{\vec{x}}$ contains the measured velocities. $A_3\hat{\vec{x}}$ gives the modeled iceberg-frame distance between DPPs, and ${}^b\vec{d}$ contains the measured (by DVL dead reckoning) iceberg-frame distance between DPPs. $A_4\hat{\vec{x}}$ encodes the loop-closure objective between relevant DPPs from the beginning and end of the circumnavigation. Finally, A_5 gives solution uniqueness by expressing a frame-centering objective.

The remainder of this section details the spline models used to represent iceberg translation and rotation, the formulation of the measurement model matrices A_i, and finally a minimization technique which handles the nonlinearity of J—specifically, that A_1, A_2, and ${}^b\vec{d}$ all depend on the unknown iceberg heading.

C. Spline Model for Iceberg Trajectory

To facilitate accurate and tractable estimation of the iceberg trajectory, the model used to express the trajectory needs to describe realistic iceberg motions using a small number of parameters compared to the total number of DVL position and velocity measurements made during data collection. Specifically, this method uses splines to represent iceberg translation and rotation through inertial space. Splines are piecewise polynomials composed of weighted sums of basis functions in time. The order, number, and spacing of basis functions may be chosen. The weights are called control points, and have a geometric interpretation. See [16] for a full coverage of splines. While a number of parametric forms (e.g., other piecewise polynomials, Fourier series) may be able to describe iceberg motion, splines are used here for three reasons:

1) splines are "well behaved" at their endpoints (versus e.g., Taylor polynomials);
2) splines allow for the inclusion of physical constraints such as continuous acceleration;
3) every position along a spline-modeled trajectory is a linear function of its control points.

This method uses one spline to represent the inertial-space trajectory taken by the origin of a reference frame attached to the iceberg ${}^I\hat{\vec{x}}_b(t)$ and another spline to represent the heading of that reference frame $\hat{\psi}_b(t)$. Both of these splines are defined in time (over the duration of data collection), and specified by a linear combination of basis splines as in

$${}^I\hat{\vec{x}}_b(t) = B_{1,D_x}(t)I\vec{P}_{x,1} + B_{2,D_x}(t)I\vec{P}_{x,2} + \cdots + B_{n,D_x}(t)I\vec{P}_{x,N_x} \quad (2)$$

$$\hat{\psi}_b(t) = B_{1,D_\psi}(t)P_{\psi,1} + B_{2,D_\psi}(t)P_{\psi,2} + \cdots + B_{n,D_\psi}(t)P_{\psi,N_\psi}. \quad (3)$$

The only free parameters in these models are the control points $\vec{P}_{x,i}$ and $P_{\psi,i}$. For a given degree D_x or D_ψ, number of control points N_x or N_ψ, and knot spacing in time, each basis spline $B_{i,D_x}(t)$ or $B_{i,D_\psi}(t)$ is a fully defined function only of time t. Note that the position spline is vector valued, while the heading spline is scalar valued.

An important property of the spline model is that both the position and velocity of the iceberg frame are described as linear functions of the same control points. Specifically, at the time of the ith measurement, the iceberg-frame position and translation rate are given by the matrix multiplications in

$$\begin{aligned} &{}^I\hat{\vec{x}}_b(t_i) \\ &\quad = [\, B_{1,D_x}(t_i)I \quad B_{2,D_x}(t_i)I \quad \ldots \quad B_{N_x,D_x}(t_i)I \,]\,\vec{P}_x \\ &\quad = B_x(t_i)\vec{P}_x \end{aligned} \quad (4)$$

$$\begin{aligned} &{}^I\hat{\dot{\vec{x}}}_b(t_i) \\ &\quad = [\, \dot{B}_{1,D_x}(t_i)I \quad \dot{B}_{2,D_x}(t_i)I \quad \ldots \quad \dot{B}_{N_x,D_x}(t_i)I \,]\,\vec{P}_x \\ &\quad = \dot{B}_x(t_i)\vec{P}_x. \end{aligned} \quad (5)$$

Importantly, the translational position and translational velocity splines differ only in their known basis functions (B versus $\dot{B}$), not in their control points.

Here, $\vec{P}_x$ is a stacked vector containing the N_x 2-D (north, east) control points for the position spline. Similarly, the modeled heading and heading rate of the iceberg are given by the matrix multiplications in

$$\begin{aligned} &\hat{\psi}_b(t_i) \\ &\quad = [\, B_{1,D_\psi}(t_i) \quad B_{2,D_\psi}(t_i) \quad \ldots \quad B_{N_\psi,D_psi}(t_i) \,]\,\vec{P}_\psi \\ &\quad = B_\psi(t_i)\vec{P}_\psi \end{aligned} \quad (6)$$

$$\begin{aligned} &\hat{\dot{\psi}}_b(t_i) \\ &\quad = [\, \dot{B}_{1,D_\psi}(t_i) \quad \dot{B}_{2,D_\psi}(t_i) \quad \ldots \quad \dot{B}_{N_x,D_\psi}(t_i) \,]\,\vec{P}_\psi \\ &\quad = \dot{B}_\psi(t_i)\vec{P}_\psi \end{aligned} \quad (7)$$

where $\vec{P}_\psi$ is a stacked vector of the scalar heading spline control points.

A small number of parameters in $\vec{P}_x$ and $\vec{P}_\psi$ completely define (through a linear model) the iceberg's translation and heading over the duration of data collection.

The modeled trajectory passes through its first and last control points. The number of inflection points in each spline curve is limited by the number of basis splines (control points) composing the curve. So, as the number and degree of the basis splines in a spline grow, so does the space of functions which the spline can accurately represent. While there is no theoretical limit on the number and degree of the basis splines used to form a spline, using more requires estimating the values of more control points and it is best to use the simplest representation which can still represent accurately the true iceberg trajectory.

The results in this paper use cubic basis splines with quadruply repeated knots at the beginning and end of data collection, and single knots at interior times, uniformly spaced in time by at most 1 h. This representation gives a spline trajectory of increasing complexity as the duration of data collection grows. Physically, the trajectory is restricted to continuous,

piecewise-linear acceleration. As a practical matter, qualitative observations of iceberg trajectory during data collection (e.g., known tidal current reversals, observed changes in wind forcing) could be used to structure the spline, but simply adding uniformly spaced single knots as the duration of data collection grows is a reliable approach with physical limitations, as described above.

D. Measurement Model Matrices

With the spline model for iceberg trajectory defined above, this section defines the measurement models used in the multiobjective least squares cost J. Since the translation spline model is linear in its control points, the vector $\hat{\vec{x}}$ appearing in (1) contains the translation spline control points and iceberg-frame DPP locations

$$\hat{\vec{x}} = \begin{bmatrix} \vec{P}_x \\ {}^b\hat{\vec{x}}_1 \\ {}^b\hat{\vec{x}}_2 \\ \vdots \\ {}^b\hat{\vec{x}}_n \end{bmatrix}. \tag{8}$$

The estimation models defined in the remainder of this section are linear functions of $\hat{\vec{x}}$.

1) Inertial-Space DPP Position: The first term in (1) is $\mu_1 \| A_1 \hat{\vec{x}} - {}^I\vec{x} \|^2$. It compares the measured inertial-space DPP positions ${}^I\vec{x}$ (which come from vehicle inertial navigation combined with DVL ranges) and the modeled inertial-space DPP positions $A_1\hat{\vec{x}}$.

The modeled inertial-space position of the ith DPP (on the iceberg surface) at the time of its measurement t_i is given by

$${}^I\hat{\vec{x}}_i(t_i) = {}^I\hat{\vec{x}}_b(t_i) + {}^{I/b}R(\hat{\psi}_b(t_i)) {}^b\hat{\vec{x}}_i \tag{9}$$

where ${}^b\hat{\vec{x}}_i$ is the position of the DPP in a reference frame attached to the iceberg, ${}^{I/b}R(\hat{\psi}_b(t_i))$ is a rotation matrix which rotates the DPP's iceberg-frame position into inertial space based on the modeled iceberg heading at the time of measurement, and ${}^I\hat{\vec{x}}_b(t_i)$ is the modeled inertial-space position of the iceberg reference frame at the time of measurement. (Note that modeled quantities are labeled with hats throughout this paper.)

Using the spline model for iceberg trajectory, (9) can be written in a matrix form as

$${}^I\hat{\vec{x}}_i(t_i) = {}^I\hat{\vec{x}}_b(t_i) + {}^{I/b}R(\hat{\psi}_b(t_i)) {}^b\hat{\vec{x}}_i = A_1\hat{\vec{x}} \tag{10}$$

where (11), shown at the bottom of the page, applies.

Note that A_1 (like A_2 and ${}^b\vec{d}$) depends on the unknown iceberg heading versus time. This nonlinearity is addressed in Section III-E.

2) Inertial-Space DPP Velocity: The second term in (1) is $\mu_2 \| A_2\hat{\vec{x}} - {}^I\dot{\vec{x}} \|^2$. It compares the measured inertial-space DPP velocities ${}^I\dot{\vec{x}}$ (which come from vehicle inertial navigation combined with DVL velocity) and the modeled inertial-space DPP velocities $A_2\hat{\vec{x}}$.

The modeled inertial-space velocity of the ith DPP, ${}^I\hat{\dot{\vec{x}}}_i$, is the sum of the modeled translational velocity of the reference frame at the time of measurement and the position-dependent velocity of the DPP due to the modeled rotation rate of the frame

$${}^I\hat{\dot{\vec{x}}}_i(t_i) = {}^I\hat{\dot{\vec{x}}}_b(t_i) + {}^{I/b}R(\hat{\psi}_b(t_i)) \left({}^b\hat{\vec{\omega}}_b(t_i) \times {}^b\hat{\vec{x}}_i \right) \tag{12}$$

where ${}^b\hat{\vec{\omega}}_b(t_i) = [\,0 \quad 0 \quad \dot{\psi}_b\,]$ is the inertial-space angular velocity of the iceberg frame, expressed in the iceberg frame.

Using the spline model of iceberg trajectory, (12) can be written in a matrix form as

$$\begin{aligned} {}^I\hat{\dot{\vec{x}}}_i(t_i) &= {}^I\hat{\dot{\vec{x}}}_b(t_i) + {}^{I/b}R(\hat{\psi}_b(t_i)) \left({}^b\hat{\vec{\omega}}_b(t_i) \times {}^b\hat{\vec{x}}_i \right) \\ &= A_2\hat{\vec{x}} \end{aligned} \tag{13}$$

where (14), shown at the bottom of the page, applies, and Ω is the skew-symmetric velocity-due-to-rotation matrix, and depends on the modeled iceberg rotation rate at each ensonification time $\hat{\dot{\psi}}_b(t_i)$.

Note that A_2 (like A_1 and ${}^b\vec{d}$) depends on the unknown iceberg heading versus time. This nonlinearity is addressed in Section III-E.

3) Iceberg-Frame Displacements Between DPPs: The third term in (1) is $\mu_3 \| A_3\hat{\vec{x}} - {}^b\vec{d} \|^2$. It compares the modeled and measured iceberg-frame displacements ($A_3\hat{\vec{x}}$ and ${}^b\vec{d}$, respectively) between sequential DPPs. Rows of A_3 are simply pairs of opposite identities such that

$$A_3 = \begin{bmatrix} 0 & \dots & -I & I & 0 & \dots \\ \vdots & \ddots & 0 & -I & I & \ddots \\ \vdots & & & \ddots & \ddots & \ddots \end{bmatrix} \tag{15}$$

and $A_3\hat{\vec{x}}$ then gives a vector of the modeled iceberg-frame displacements between sequential DPPs.

The measured iceberg-frame displacements between sequential DPPs, ${}^b\vec{d}_i$, are dead reckoned in the iceberg frame according

$$A_1 = \begin{bmatrix} B_x(t_1) & {}^{I/b}R(\hat{\psi}_b(t_1)) & 0 & \dots & 0 \\ B_x(t_2) & 0 & {}^{I/b}R(\hat{\psi}_b(t_2)) & \dots & 0 \\ \vdots & \vdots & \vdots & \ddots & \vdots \\ B_x(t_n) & 0 & 0 & \dots & {}^{I/b}R(\hat{\psi}_b(t_n)) \end{bmatrix}. \tag{11}$$

$$A_2 = \begin{bmatrix} \dot{B}_x(t_1) & {}^{I/b}R(\hat{\psi}_b(t_1))\Omega(\hat{\dot{\psi}}_b(t_1)) & 0 & \dots & 0 \\ \dot{B}_x(t_2) & 0 & {}^{I/b}R(\hat{\psi}_b(t_2))\Omega(\hat{\dot{\psi}}_b(t_2)) & \dots & 0 \\ \vdots & \vdots & \vdots & \ddots & \vdots \\ \dot{B}_x(t_n) & 0 & 0 & \dots & {}^{I/b}R(\hat{\psi}_b(t_n))\Omega(\hat{\dot{\psi}}_b(t_n)) \end{bmatrix} \tag{14}$$

to the DVL-measured iceberg-relative vehicle velocities and the iceberg-relative vehicle headings. Importantly, the iceberg-relative vehicle heading at the time of each measurement depends on both the measured vehicle heading and the estimated iceberg heading. Each row of ${}^b\vec{d}$ is computed as

$$ {}^b\vec{d}_i = -{}^{b/v}R(t_{i-1})\,{}^v\vec{r}_{i-1} + \sum_k {}^{b/v}R(t_k)\,{}^v\dot{\vec{x}}_{v/b}(t_k)\Delta t_k + {}^{b/v}R(t_i)({}^v\vec{r}_i) \quad (16) $$

where each rotation matrix from the vehicle frame to the iceberg frame ${}^{b/v}R(t)$ is computed based on the measured vehicle heading and the estimated iceberg heading at time t, ${}^v\dot{\vec{x}}_{v/b}$ is the DVL-measured iceberg-relative vehicle velocity (defined in the vehicle frame), Δt is the time between DVL velocity measurements, ${}^v\vec{r}$ are DVL-measured range vectors from the vehicle to a DPP, and t is time. Indices i and $i-1$ refer to sequential DPPs and their associated measurement times, while k indexes DVL velocity measurements collected between the ith and $(i-1)$th DPPs (including the velocity measurement from the ith DPP).

The three terms of (16) give the distance from the $(i-1)$th DPP to the vehicle at the time it was measured, plus the (zeroth-order-hold) velocity-dead-reckoned distance traveled by the vehicle from then until the ith DPP, plus the distance from the vehicle to the ith DPP at the time it was measured. The key is that heading information for the dead-reckoned distance comes from both the vehicle inertial heading reference and the estimated iceberg heading at the time of each measurement.

The multiobjective least squares minimization of J involves computing the pseudoinverse of a highly structured matrix. However, the size of this matrix is at least $6n \times n$, where n is the number of DPPs used. A DVL pinging at 5 Hz during a 1-h circumnavigation collects 18 000 position and velocity measurements. The important dead-reckoned distance between DPPs is computed from all the collected DVL measurements, so not every one needs to be assigned a DPP to achieve good mapping performance. The DPPs used should be spread out evenly around the iceberg. As fewer DPPs are used, the uncertainty in the dead-reckoned displacement between them grows. The number of DPPs should be chosen such that this uncertainty remains less than the desired mapping performance (longer computation time results from using more DPPs). DVL dead reckoning is typically capable of accuracy better than 1% of distance traveled for vehicles traveling at speeds around 1.5 m/s [9]. The results presented in Section IV-A use a DPP spacing of 22.5 m, and a simulated DVL dead-reckoning error growth rate of approximately 0.4% of distance traveled.

As an aside, note that adding a 3-D imaging sonar, or an additional multibeam sonar scanning in a horizontal fan, could provide additional iceberg-frame displacement measurements through some form of iterative closest point (ICP) alignment between sequential, overlapping sonar "images." In areas of sufficient iceberg texture for ICP, these methods could give full 6-D vehicle displacements between pings, while in degenerate geometries (e.g., along planar walls), they could still provide iceberg-relative vehicle heading information. As is, the estimation does not require 3-D sonar or an additional horizontal multibeam sonar for iceberg-relative heading measurement.

4) Loop Closure: The fourth term in (1) is $\mu_4\|A_4\hat{\vec{x}}\|^2$. It represents the squared iceberg-frame distances between modeled DPP positions observed at the end of the circumnavigation and their corresponding loop-closure locations from the beginning of the circumnavigation.

Prior work simply chose a constant iceberg velocity and rotation rate to best satisfy loop closure based on alignment of the multibeam sonar point clouds from the beginning and end of the circumnavigation. In the present method, loop closure is still utilized, but in a manner consistent with the parameters to be identified.

Loop closure is determined by alignment of multibeam ranges from the beginning and end of the circumnavigation. This can be performed using projective methods such as those available in MB-System [6], or by the ICP method [3], or by a more general search such as that in [11] (where loop closure is achieved by minimizing the sum of squared nearest neighbor distances between overlapping multibeam ranges collected at the beginning and end of the circumnavigation).

To be considered with the rest of the objectives, the loop-closure alignment of the multibeam data must be expressed in terms of $\hat{\vec{x}}$. This is straightforward since the multibeam sonar and DVL range vectors are both defined in the vehicle frame. In general, multibeam alignment will reveal that the position of some kth DPP from the end of the circumnavigation lies a fractional distance, $0 < z < 1$, between the positions of two successive DPPs p and q from the beginning of the circumnavigation

$$ {}^b\vec{x}_k \approx (1-z)\,{}^b\vec{x}_p + z\,{}^b\vec{x}_q. \quad (17) $$

This is a polygonal approximation to the iceberg surface. However, DVLs generally operate with high enough sampling rate (usually >5 Hz) that the approximation is a very good one.

The loop-closure matrix A_4 contains one row for each group of DPPs whose iceberg frame positions may be expressed in this way

$$ A_4 = \begin{bmatrix} 0 & \dots & (1-z)I & zI & 0 & \dots & 0 & -I & 0 & \dots \\ \vdots & \ddots & & \ddots & \ddots & \ddots & \ddots & \ddots & \ddots & \ddots \end{bmatrix}. \quad (18) $$

Minimizing the norm $\|A_4\hat{\vec{x}}\|^2$ satisfies loop closure.

5) Solution Uniqueness: The fifth term in (1) is $\mu_5\|A_5\hat{\vec{x}}\|^2$. It assigns a preference that the iceberg reference frame have its origin at the mean of the modeled DPP positions. There is an infinite family of solutions that minimize the first four norms since the iceberg-fixed frame origin may be placed arbitrarily (even off the iceberg) so long as it moves with the iceberg, and the spline trajectory describes its motion accordingly. Using

$$ A_5 = [\,0 \quad \dots \quad I \quad \dots\,] \quad (19) $$

the fifth norm in (1) serves to center the reference frame geometrically on the iceberg, yielding a unique solution.

E. Solution Technique

The cost J [see (1)] is nonlinear in terms of the quantities being estimated because A_1, A_2, and $\vec{d}$ all depend on the un-

known iceberg heading over time. However, the cost function is linear in the remaining parameters. Exploiting this, the function is minimized using an outer loop search over the small number of iceberg heading spline control points and a fast, linear least squares inner loop over the vast majority of estimation parameters including iceberg translation spline control points and iceberg-frame positions of the DPPs.

Each computation by the inner loop treats the iceberg heading trajectory defined by the outer loop as "known." For each outer loop iteration, A_1, A_2, and ${}^b\vec{d}$ are computed anew and used in a simple linear least squares computation to minimize J over the iceberg translation spline parameters and iceberg-frame DPP positions. The least squares residual $\|A\hat{\vec{x}}_{ls} - b\|$ from the inner loop is then used by the outer loop to search the space of iceberg heading spline control points. This solution structure is shown in Fig. 4, where

$$A = \begin{bmatrix} A_1 \\ \sqrt{\mu_2}A_2 \\ \sqrt{\mu_3}A_3 \\ \sqrt{\mu_4}A_4 \\ \sqrt{\mu_5}A_5 \end{bmatrix}, \quad b = \begin{bmatrix} {}^I\vec{x} \\ \sqrt{\mu_2}{}^I\dot{\vec{x}} \\ \sqrt{\mu_3}{}^b\vec{d} \\ 0 \\ 0 \end{bmatrix}, \quad \text{and} \quad \hat{\vec{x}}_{ls} = A^{\dagger}b. \tag{20}$$

The task of the outer loop is to find the iceberg heading trajectory (heading versus time) which yields the lowest least squares residual in the inner loop. Because the outer loop must search over only a small number of parameters (approximately two or three for every hour of data collection), it can be implemented using a number of search techniques including simplex and even exhaustive methods. The results shown in Sections IV-A and IV-B were obtained using a simplex search for the outer loop parameters. It is possible that the entire model formulation could be adapted to fit some existing nonlinear least squares solvers.

The weighting values μ_1 through μ_5 are chosen based on the quality of the sensor data they multiply and the relative magnitudes of errors to be penalized depending on units used. Specifically

$$\mu_1 = 1, \quad \mu_i = z_1^2/z_i^2 \tag{21}$$

where z_i is the uncertainty in the ith measurement. This method is in the spirit of Bryson's rule for selecting linear quadratic regulator (LQR) weights [4]. The relative sizes of the weights will change the result accordingly to fit better the highest weighted terms.

For the simulated results in Section IV-A, the inertial-space DPP positions are measured with approximately 76-m root mean square (RMS) error (after GPS fixing), while the dead-reckoned displacements between DPPs are measured with approximately 0.04-m RMS error. The inertial-space DPP velocities are measured with approximately 0.007-m/s RMS error. Taking these RMS values as z_i gives order-of-magnitude weights $\mu_1 = 1$, $\mu_2 = 1e8$, and $\mu_3 = 4e6$. Simulation has shown that these weights may be varied by at least two orders of magnitude without substantially affecting mapping results. The loop-closure weight μ_4 is chosen based on the uncertainty in multibeam alignment of loop-closure DPPs, but also based on the number of loop-closure DPPs, to give a total cost contribution on the order of the other terms. In the simulation results, there are eight loop-closure DPPs (of 158 total), located with better than 10-cm RMS error, and μ_4 is chosen to be $1e10$. The frame-centering solution uniqueness weight is chosen to be very small so that it will not degrade performance for iceberg trajectories in which the geometric center of the iceberg does not follow exactly a spline-describable trajectory: $\mu_5 = 1e-10$. Simulation has shown that the weights μ_4 and μ_5 may be changed by two to three orders of magnitude without substantially affecting mapping results.

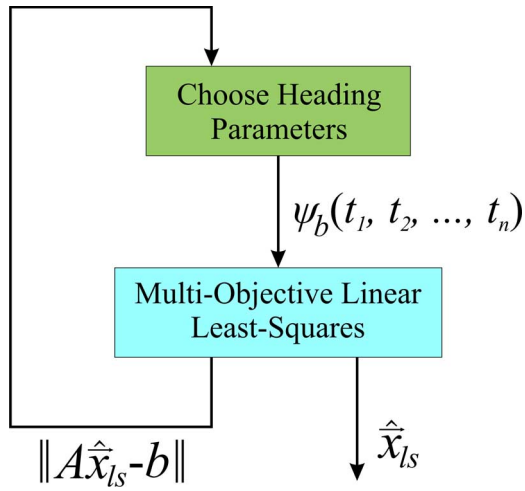

Fig. 4. Estimation is separated into an outer loop over iceberg heading, and a fast, linear least squares inner loop over iceberg translational trajectory and DPP positions.

Once the optimization has been solved, the final steps in making the map are to compute the iceberg-relative AUV trajectory from the estimated DPP positions and estimated iceberg heading, and to project the recorded multibeam ranges from that trajectory.

IV. Results

Currently, iceberg circumnavigation data from a submerged vehicle with DVL and multibeam sonar are unavailable. The ship-based data in Fig. 1 include only vehicle inertial navigation and multibeam sonar—they do not include DVL velocities [12], and so cannot be used in validating the extended method presented in this paper. This section presents mapping results from two different data sources:

1) planar simulation of a free-drifting iceberg;
2) AUV data collected over the seafloor from a closed-loop trajectory.

The simulation data provide a moving iceberg testbed with known ground truth for the mapping results. Although the seafloor data lack map ground truth, the trajectory of the seafloor is known to be stationary, and demonstrating that the method estimates a stationary trajectory for the seafloor given high-quality inertial navigation serves as an important verification of the method with real vehicle and instrument data.

A. Simulation Results

Simulation of circumnavigation data from a moving iceberg allows for direct comparison of iceberg mapping results with ground truth. It allows the complexity of the iceberg trajectory

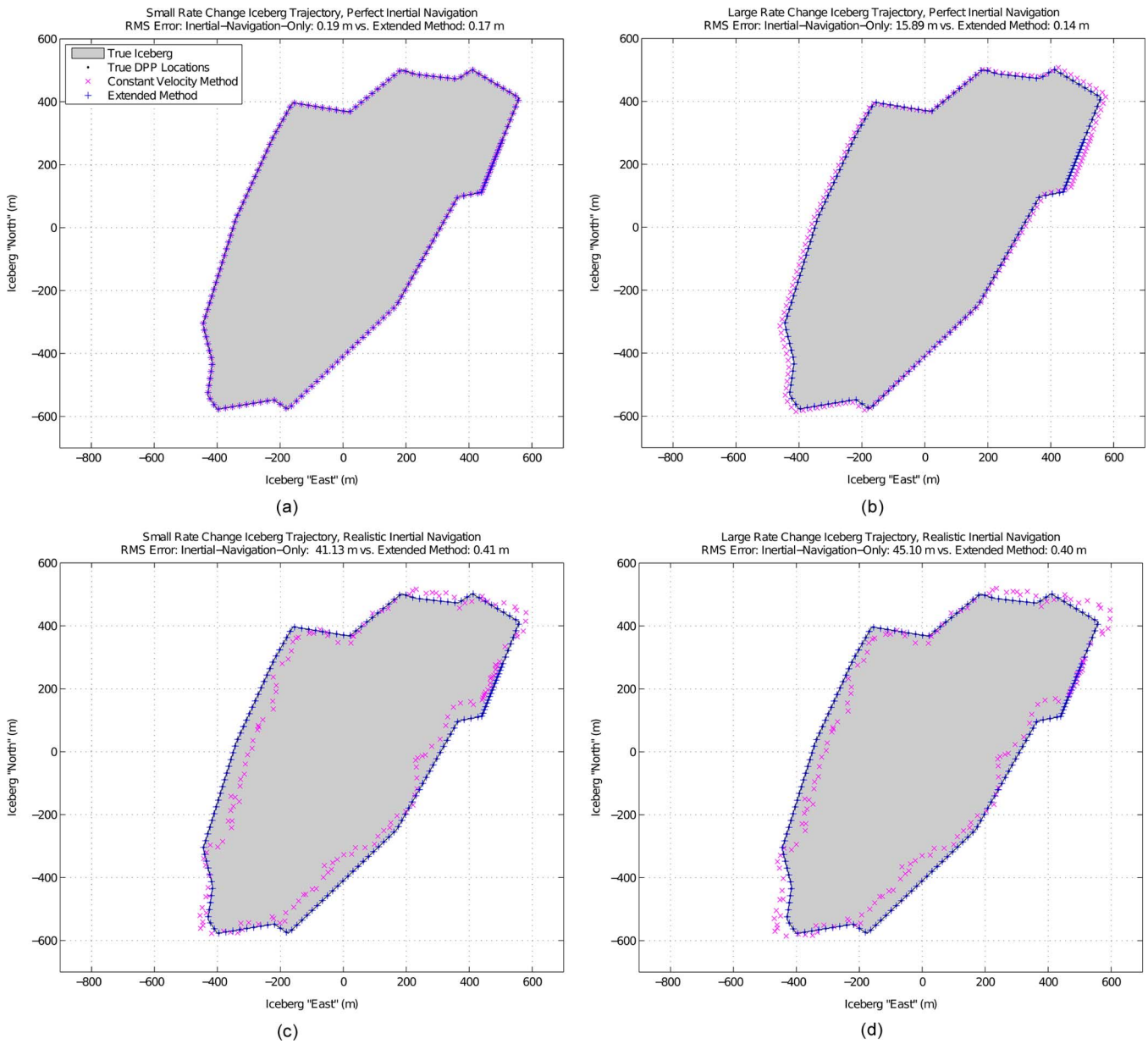

Fig. 5. Simulated iceberg mapping results are demonstrated for small and large rate change iceberg trajectories, as well as for perfect and realistic inertial navigation measurements. Results are shown with RMS mapping errors from the constant-velocity method of [12] and the extended method presented in this paper.

as well as the quality of available measurements to be varied, and allows for evaluation of the mapping performance versus these parameters.

Fig. 5 presents a matrix of mapping results. The top two plots use perfect vehicle inertial navigation, while the bottom two plots use vehicle inertial navigation with realistic errors (i.e., drift and noise). The left two plots use a nearly constant rate iceberg trajectory, while the right two plots use an iceberg trajectory with rapidly changing (but still realistic) translation and rotation rates. The iceberg-relative vehicle trajectory and DPP locations are identical for all four cases.

The title of each pane includes the RMS mapping error over all the retained DPPs versus ground truth for both the method presented in this paper (called the "extended method" in the figure) and a constant-velocity method with no DVL measurements, equivalent to the method in [12]. The primary message of Fig. 5 is that both degraded inertial navigation quality and increased variability in iceberg translation and rotation rates have significant detrimental impacts on the mapping performance of the inertial-navigation-only method, while the extended method is robust to these factors. The *exact* RMS mapping error due to each factor depends on the specific iceberg trajectory and on the error characteristics of the specific vehicle sensors, but the values used in the simulation are representative of common AUV sensors and plausible iceberg trajectories. For reference, the small and large rate change simulated trajectories used to generate Fig. 5 appear in Fig. 6.

1) Simulation Details: The simulated vehicle circumnavigates the 3364.7-m perimeter iceberg 1.05 times over 39.25 min at a constant iceberg-relative velocity of 1.5 m/s. The simulated DVL measurement rate is 10 Hz, giving 23 552 measurements, of which 158 (every 150th) are assigned a DPP in the optimiza-

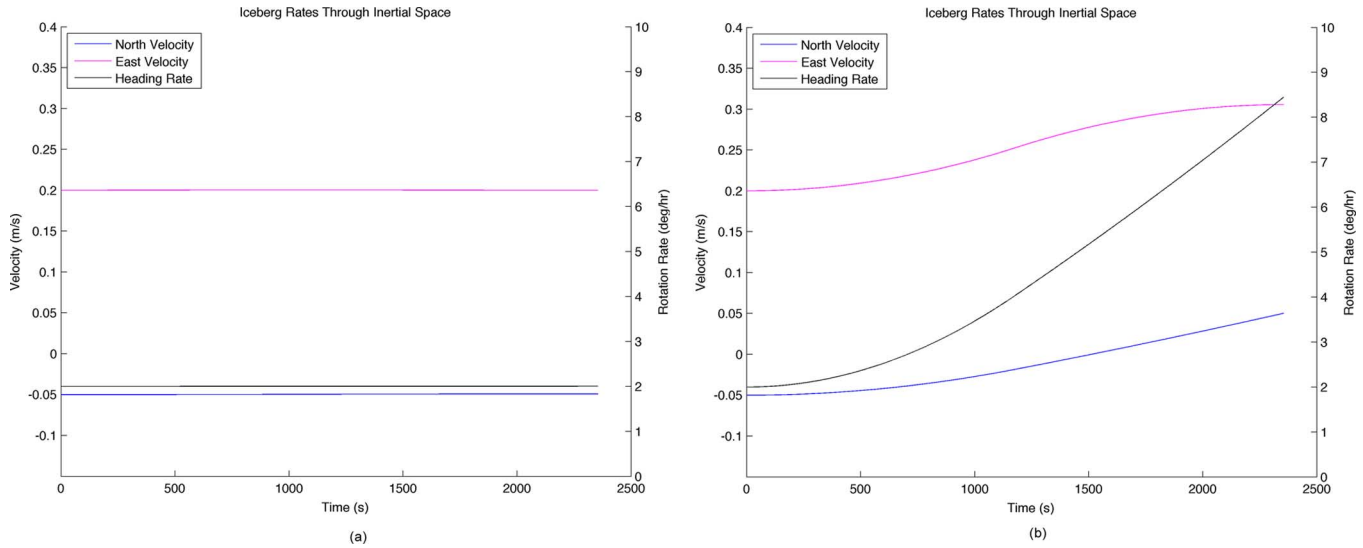

Fig. 6. Translation and rotation rates from the two simulated iceberg trajectories are plotted on the same scales. (a) Small rate change trajectory. (b) Large rate change trajectory.

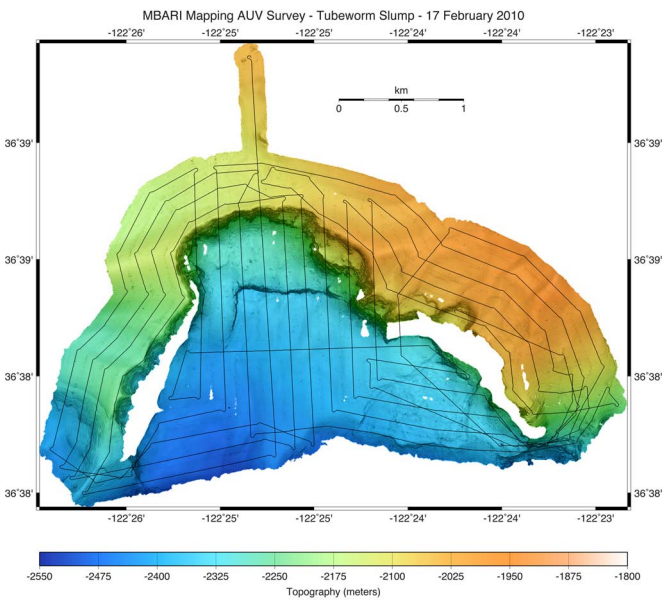

Fig. 7. Trajectory of the mapping vehicle over Tubeworm Slump.

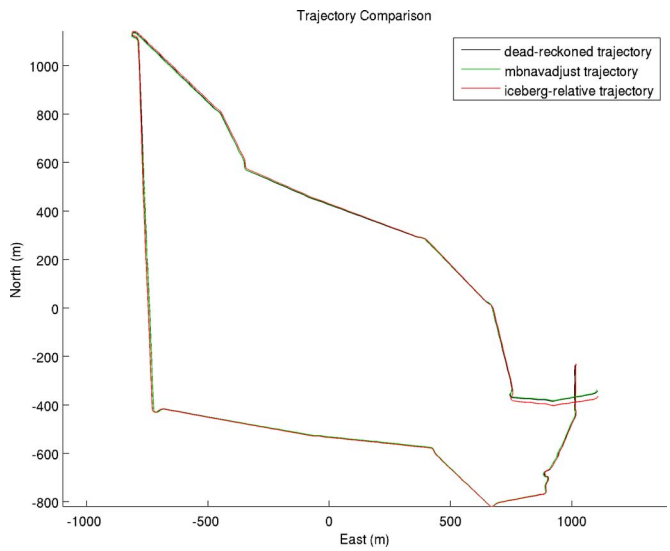

Fig. 8. Despite its iceberg-trajectory-free parameters, the iceberg mapping method estimates a seafloor-relative trajectory for the AUV very similar to that estimated by existing methods.

tion (as described in Section III-D3), including eight loop-closure DPPs from the end of the circumnavigation. Simulated realistic vehicle inertial navigation error is the same for both iceberg trajectories, reaching 1055 m by the end of the circumnavigation. However, the inertial navigation trajectory used by both methods is "fixed" by linear smoothing using simulated deployment and recovery (error-free) GPS locations. The corrected inertial-space trajectory has zero error at the beginning and end, and reaches a maximum error of 74.6 m at 17.1 min into the data collection. Dead-reckoned displacements between DPPs are measured with approximately 0.05-m RMS error, due to 0.002-m/s DVL bias velocity, and (0, 0.005) Gaussian noise corrupting velocity measurements. The inertial-space DPP velocities are measured with approximately 0.007-m/s RMS error. The extended method in the simulation uses $\mu_1 = 1$, $\mu_2 = 1e7$, $\mu_3 = 1e6$, $\mu_4 = 1e10$, and $\mu_5 = 1e - 10$, but these can be changed by one or two orders of magnitude without substantially changing the mapping performance (e.g., RMS errors for the extended method remain less than 10 m). The heading and translation splines are each cubic with quadruply repeated knots at end times, and one internal knot. The five heading spline control points are initialized to all zeros. The first is held at zero, and the search over the remaining four heading spline control points converges within 15–20 iterations of a simplex search (requiring 105–130 inner loop computations) for all of the presented data sets.

Since the RMS mapping errors depend on representative, but invented, simulation parameters, and on the specific realizations of measurement noise, their approximate magnitudes are more important than their *exact* values.

B. Experimental Results

Although DVL and multibeam data from an AUV circumnavigation of a free-drifting iceberg are presently unavailable,

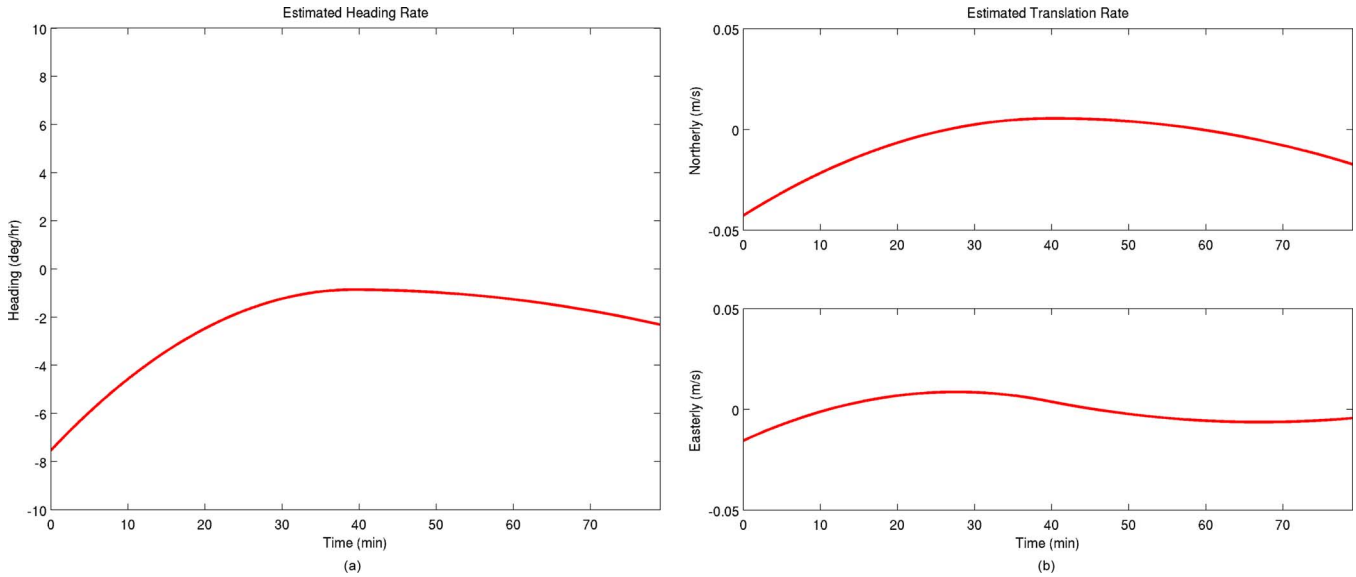

Fig. 9. Method estimates heading and translation rates near zero for the seafloor surrogate "iceberg."

it is valuable to verify performance of the mapping method using real AUV data. This section presents successful mapping results from a fully autonomous submerged AUV demonstration in which the vehicle ensonified the seafloor using downward-looking sonar. Even though the seafloor is stationary, it is treated as an "iceberg" with unknown motion—its trajectory must be accounted for in the estimation.

The data set used for this demonstration was collected during AUV mapping operations at Tubeworm Slump in Monterey Canyon. The site is a roughly 100-m-deep depression along the side of the main canyon. The trajectory flown by the mapping vehicle was designed to obtain complete sonar coverage of the site. It appears along with the underlying bathymetry in Fig. 7.

The demonstration presented here uses only a single self-intersecting portion of the data from the Eastern half of the mapped area. This single loop represents a surrogate iceberg circumnavigation. It was completed in 88 min at an average altitude of 55 m, and comprises 8595 DVL measurements, of which 717 (every 12th measurement) are assigned a DPP in the optimization (as described in Section III-D3).

The demonstration lacks mapping ground truth, but comparison with seafloor mapping results from traditional methods provides qualitative verification of the mapping results from the iceberg method. Fig. 8 shows the seafloor-relative vehicle trajectory estimated by bottom-lock DVL dead reckoning, by MBSystem using mbnavadjust (a traditional seafloor mapping method), and by the iceberg mapping method. The figure shows that despite its iceberg-trajectory-free parameters (and the iceberg heading rate being initialized to 60°/h), the iceberg mapping method converges to an estimate of seafloor-relative AUV trajectory that agrees (typically within 5 m) with that determined by existing seafloor mapping methods.

Just as in the simulation results, the translation and rotation spline models used here to represent iceberg motion all have five control points (nine knots, with the first and last knot having multiplicity 4), spaced evenly by 22 min. Recall from Section III-E that this means the algorithm's inner loop performs a linear least squares estimate over $2 \times 5 + 2 \times 717$ parameters, while the outer loop searches the (small) 5-D space of heading spline control points. The outer loop is initialized to a (far from truth) constant heading rate of 60°/h. (Equivalent results are also achieved from an initialized heading rate of $-60°$/h.) The multiobjective weights are $\mu_1 = 1$, $\mu_2 = 1e4$, $\mu_3 = 1e-10$, $\mu_4 = 1e16$, and $\mu_5 = 1e-6$.

Note that the experimental results use a value of μ_4 four orders of magnitude smaller than the other weights. Because this situation involves a constant-rate iceberg trajectory (stationary), and very high-quality vehicle inertial navigation (from bottom-lock DVL), increasing μ_4 does not substantially improve mapping accuracy. Again, exact mapping ground truths are note available from the field data to evaluate this tradeoff.

1) The Inertial-Space "Iceberg" Trajectory: Use of the seafloor as a surrogate iceberg means that the "iceberg's" inertial-space trajectory is known to be exactly stationary. The inertial-space iceberg trajectory spline control points are intermediate variables in the mapping method, but it is interesting to compare the estimated trajectory with known ground truth in the case of the seafloor surrogate "iceberg." Even though the outer loop over iceberg heading was initialized far from truth with a heading rate of 60°/h, the algorithm converged to a nearly stationary estimate of the trajectory in both heading and translation. The estimated "iceberg" trajectory rates are plotted in Fig. 9. They are generally less than 4°/h, and 3 cm/s, respectively.

2) Possible Error Sources: The experimental results provide a "sanity check" on the algorithm performance with real data. The small deviations from an exactly stationary trajectory indicate loop closure and vehicle sensor bias as potential sources of error.

Although the trajectory is self-intersecting, it is only self-intersecting at a single point. Circumnavigation trajectories that are self-intersecting and parallel for some finite length (e.g., at least 5–10 m) allow multiple loop-closure DPPs to be identified and expressed in A_4. Here, the trajectory is self-intersecting at only a single point, and just one pair of DPPs is used to define loop closure. The DPPs used are the two DPPs closest to

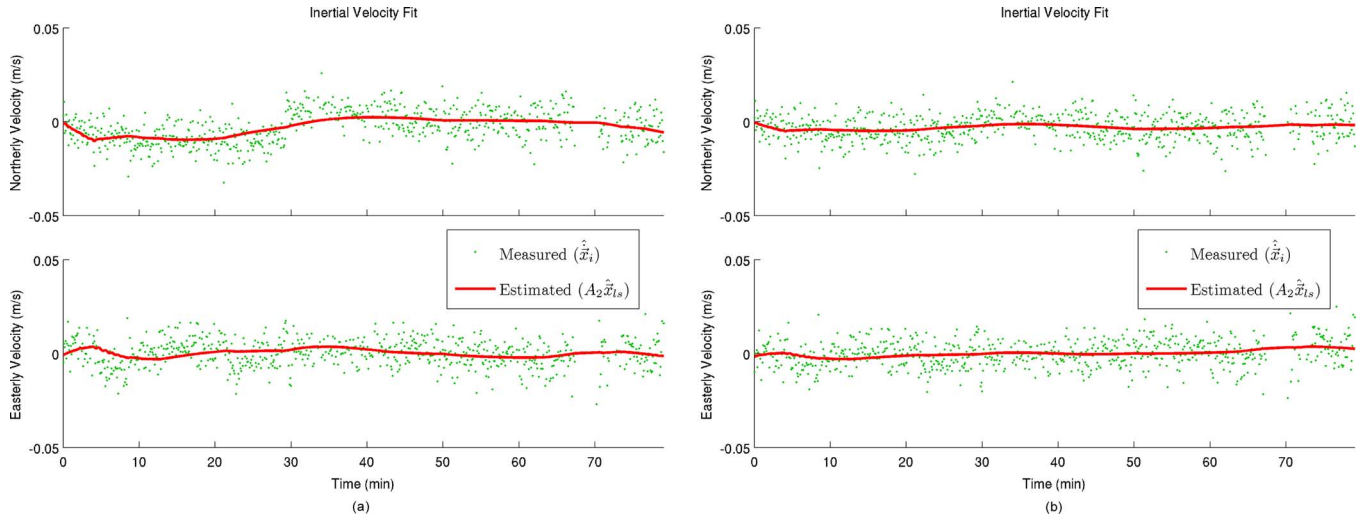

Fig. 10. Inertial-space DPP velocities are shown (a) without and (b) with DVL bias correction. Since the seafloor is known to be stationary, these data should be zero-mean.

one another in inertial space from the beginning and end of the circumnavigation. Further, since the beginning and end of the trajectory are approximately orthogonal, the formulation of A_4 as described in Section III-D4 is inappropriate for this data set. Here, A_4 is implemented as one block row of all zeros other than two opposite identities, one for each of the two loop-closure DPPs. This is a source of error since those two DPP locations actually lie several meters apart on the seafloor. A_4 could be reformulated to express loop closure at a single intersection point exactly, but that point would be ill-defined for parallel, overlapping trajectory segments (such as those along a vertical face, passed twice at constant depth and standoff distance).

Expressed in the vehicle frame, the measured inertial-space DPP velocities are not zero mean, but are nearly constant mean. The mean magnitudes are -0.0039 m/s in vehicle fore/aft, -0.0029 m/s in vehicle starboard/port, and 0.0023 m/s in vehicle down/up. These velocities are consistent with typical DVL bias velocities (e.g., [9]), and subtracting these values from the raw measured velocities before they are rotated into inertial space for use in the mapping method improves estimation performance.

Fig. 10 shows in green ${}^I\hat{\dot{x}}_i$, the measured inertial-space DPP velocities expressed in inertial space, without and with the simple correction by vehicle-frame bias subtraction. Note that the sudden change in mean apparent in the uncorrected velocities is not apparent in the corrected measured velocities. The solid red curve connects the estimated inertial-space DPP velocities $(A_2\hat{\dot{x}}_{ls})$, and shows how well the model matches the measurements for this one objective. Estimated iceberg rates using the bias-corrected inertial-space velocities are roughly half of those shown in Fig. 9—generally less than 2°/h in heading, and 1.5 cm/s in translation.

The bias velocity correction as performed here is possible because the terrain is known in advance to be stationary. However, it indicates gains to be had from a slight reformulation of the estimation routine to include vehicle-frame bias velocities as parameters to be estimated. Operationally, this may require maneuvers during data acquisition to ensure observability of the bias rates.

Biases in other sensors (e.g., compass calibration), and errors in their installation offsets (e.g., used in lever corrections, and frame rotations) represent additional sources of error in the post-processing solution not accounted for in the method.

V. Summary and Conclusion

This paper presents a technique for mapping a moving iceberg using an AUV. The key technical feature of the work is a method for estimating simultaneously the translation, rotation, and shape of an iceberg based on typical mapping data collected during a circumnavigation.

The method uses splines to parameterize both the translation and heading trajectories of the iceberg. The orders of the splines as well as the numbers of control points used to define them may be varied to describe iceberg motion up to physically meaningful constraints such as continuous piecewise-linear acceleration, and a maximum number of inflection points in iceberg trajectory.

The method chooses simultaneously spline control point values and the locations of DVL measurements in an iceberg-fixed reference frame to maximize consistency with collected data. The data include inertial-space positions and velocities of points on the iceberg surface (from DVL ranges and velocities, and vehicle inertial navigation), iceberg-frame displacements between DVL measurements, and loop-closure between the beginning and end of data collection (from overlapping sets of multibeam sonar ranges).

Modeled values of the collected data are nonlinear in iceberg heading spline parameters, but linear in the iceberg translation spline parameters and in the iceberg-frame measurement locations. To find the best estimate, an outer loop performs an iterative search over the relatively small space (on the order of ten dimensions) of heading trajectory spline control points, while a fast, linear least squares inner loop calculation solves for the optimal values of the iceberg translation spline control points and iceberg-frame DVL measurement locations (on the order of tens of thousands of dimensions).

In addition to the method itself, the paper presents mapping results from simulated free-drifting iceberg data as well as

from a seafloor surrogate iceberg data set collected by an AUV at Tubeworm Slump in Monterey Canyon. Mapping results from the simulated data illustrate the mapping performance of the method versus ground truth, and specifically demonstrate the method's robustness to errors in vehicle inertial navigation and to variable-rate iceberg trajectories. The results from field data demonstrate that the solution technique achieves a good estimate of iceberg trajectory even after poor initialization. They also point toward identification of vehicle sensor bias as a worthwhile extension of the method.

Finally, note that this technique could be adapted to other moving-environment mapping applications such as offshore assets, ship hulls, and asteroids.

Acknowledgment

The authors would like to thank D. Caress for his help with MBSystem and for providing the Tubeworm Slump data set and access to the Monterey Bay Aquarium Research Institute (MBARI, Moss Landing, CA, USA) mapping AUV, its sensors, and specifications.

References

[1] S. Augenstein and S. Rock, "Improved frame-to-frame pose tracking during vision-only SLAM/SFM with a tumbling target," in *Proc. IEEE Int. Conf. Robot. Autom.*, Shanghai, China, May 2011, pp. 3131–3138.

[2] J. Bellingham, C. Goudey, T. Consi, J. Bales, D. Atwood, J. Leonard, and C. Chryssostomidis, AUV Technology, "A second generation survey AUV," in *Proc. Symp. Autonom. Underwater Veh. Technol.*, Jul. 1994, pp. 148–155.

[3] P. Besl and N. McKay, "A method for registration of 3-D shapes," *IEEE Trans. Pattern Anal. Mach. Intell.*, vol. 14, no. 2, pp. 239–256, Feb. 1992.

[4] A. Bryson and Y. Ho, *Applied Optimal Control*. Waltham, MA, USA: Blaisdell, 1969, ch. 5.

[5] Canadian Hydraulics Centre, National Research Council of Canada, "Techniques for determining the maximum draft of an iceberg," Canadian Seabed Research Ltd., Axiom Engineering Ltd., and Cormorant Ltd., Ottawa, ON, Canada, Tech. Rep. PERD/CHC 20-46, Mar. 2000.

[6] D. Caress and D. Chayes, "MB-System: Seafloor mapping software," Open Source Software Distributed From the MBARI and L-DEO Web Sites, 2013 [Online]. Available: http://www.mbari.org/data/mbsystem/

[7] V. Ferrini, D. Fornari, T. Shank, J. Kinsey, M. Tivey, S. Soule, S. Carbotte, L. Whitcomb, D. Yoerger, and J. Howland, "Submeter bathymetric mapping of volcanic and hydrothermal features on the East Pacific Rise crest at 950 °N," *Geochem. Geophys. Geosyst.*, vol. 8, no. 1, Jan. 2007, DOI: 10.1029/2006GC001333.

[8] R. Gladstone and G. R. Bigg, "Satellite tracking of icebergs in the Weddell Sea," *Antarctic Sci.*, vol. 14, no. 3, pp. 278–287, 2002.

[9] Teledyne RD Instruments, "Workhorse navigator datasheet," Tech. Rep. Rev., Jul. 20–21, 2006.

[10] M. Jakuba, C. Roman, H. Singh, C. Murphy, C. Kunz, C. Willis, T. Sato, and R. Sohn, "Long-baseline acoustic navigation for under-ice autonomous underwater vehicle operations," *J. Field Robot.*, vol. 25, no. 11-12, pp. 861–879, 2008.

[11] P. Kimball and S. Rock, "Sonar-based iceberg-relative AUV navigation," in *Proc. IEEE/OES Autonom. Underwater Veh.*, Woods Hole, MA, USA, Oct. 2008, DOI: 10.1109/AUV.2008.5290534.

[12] P. Kimball and S. Rock, "Sonar-based iceberg-relative navigation for autonomous underwater vehicles," *Deep Sea Res. II, Top. Studies Oceanogr.*, vol. 58, no. 11-12, pp. 1301–1310, 2011.

[13] W. Kirkwood, "Development of the DORADO mapping vehicle for multibeam, subbottom, and sidescan science missions: Research Articles," *J. Field Robot.*, vol. 24, no. 6, pp. 487–495, 2007.

[14] C. Kunz, "AUV navigation and mapping in dynamic, unstructured environments," Ph.D. dissertation, Joint Program Appl. Ocean Sci. Eng., Massachusetts Inst. Technol./Woods Hole Oceanogr. Inst., Cambridge/Woods Hole, MA, USA, Nov. 2011.

[15] P. R. McGill, K. R. Reisenbichler, S. A. Etchemendy, T. C. Dawe, and B. W. Hobson, "Aerial surveys and tagging of freedrifting icebergs using an unmanned aerial vehicle (UAV)," *Deep Sea Res. II, Top. Studies Oceanogr.*, vol. 58, no. 11, pp. 1318–1326, 2011.

[16] L. Piegl and W. Tiller, *The NURBS Book*. New York, NY, USA: Springer-Verlag, Jan. 1997.

[17] C. Roman and H. Singh, "Improved vehicle based multibeam bathymetry using sub-maps and SLAM," in *Proc. IEEE/RSJ Int. Conf. Intell. Robots Syst.*, Aug. 2005, pp. 3662–3669.

[18] P. Wadhams and M. Kristensen, "The response of antarctic icebergs to ocean waves," *J. Geophys. Res.*, vol. 88, no. C10, pp. 6053–6065, 1983.

[19] D. Yoerger, M. Jakuba, and A. Bradley, "Techniques for deep sea near bottom survey using an autonomous underwater vehicle," *Int. J. Robot. Res.*, vol. 26, no. 1, pp. 41–54, Jan. 2007.

Peter W. Kimball received the Ph.D. degree in aeronautics and astronautics from Stanford University, Stanford, CA, USA, in August 2011.

He has been with the Woods Hole Oceanographic Institution, Woods Hole, MA, USA, on a postdoctoral scholarship, since April 2013. His research interests include navigation, control, operation, and data analysis techniques for autonomous robots.

Stephen M. Rock received the S.B. and S.M. degrees in mechanical engineering from the Massachusetts Institute of Technology (MIT), Cambridge, MA, USA, in 1972 and the Ph.D. degree in applied mechanics from Stanford University, Stanford, CA, USA, in 1978.

He is a Professor in the Department of Aeronautics and Astronautics and the Director of the Aerospace Robotics Laboratory, Stanford University, Stanford, CA, USA. He is also an adjunct at the Monterey Bay Aquarium Research Institute (MBARI), Moss Landing, CA, USA. He joined the Stanford faculty in 1988. Before that, he led the Controls and Instrumentation Department, Systems Control Technology, Inc. His interests include the development and experimental verification of advanced navigation and control techniques for space and underwater autonomous robotic vehicle systems.

Dr. Rock is a Fellow of the American Institute of Aeronautics and Astronautics (AIAA).